Article

Hydroxy-Terminated Organic Semiconductor-Based Field-Effect Transistors for Phosphonate Vapor Detection

Jia Huang, Joseph Miragliotta, Alan Becknell, and Howard E. Katz

J. Am. Chem. Soc., **2007**, 129 (30), 9366-9376• DOI: 10.1021/ja068964z • Publication Date (Web): 11 July 2007

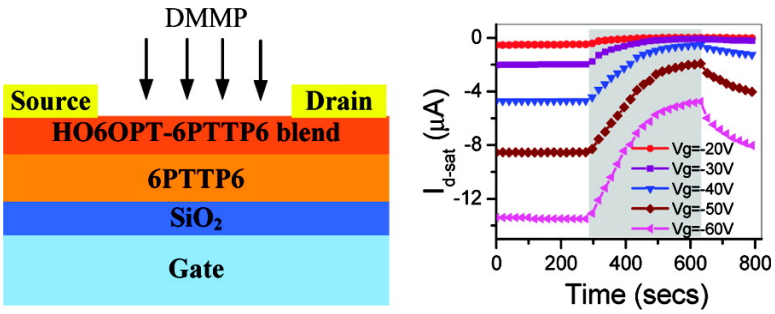

More About This Article

Additional resources and features associated with this article are available within the HTML version:

- Supporting Information
- Links to the 11 articles that cite this article, as of the time of this article download
- Access to high resolution figures
- Links to articles and content related to this article
- Copyright permission to reproduce figures and/or text from this article

View the Full Text HTML

J|A|C|S
ARTICLES
Published on Web 07/11/2007

Hydroxy-Terminated Organic Semiconductor-Based Field-Effect Transistors for Phosphonate Vapor Detection

Jia Huang,[†] Joseph Miragliotta,[‡] Alan Becknell,[‡] and Howard E. Katz*,[†]

Contribution from the Department of Materials Science and Engineering, Johns Hopkins University, Baltimore, Maryland 21218, and Sensor system group, Research and Technology Development Center, Applied Physics Laboratory, The Johns Hopkins University, Laurel, Maryland 20723

Received December 14, 2006; E-mail: hekatz@jhu.edu

Abstract: Organic field-effect transistors (OFETs) with a hydroxy-functionalized semiconductor incorporated into a receptor layer were fabricated and shown to respond strongly to the analyte dimethyl methylphosphonate (DMMP) that simulates phosphonate nerve agents. Large and reproducible source−drain current changes were observed upon exposure to DMMP vapor. Compared to single component transistors, OFETs with a mixed hydroxylated and nonhydroxylated semiconductor upper layer exhibited higher sensitivity. We further investigated the selectivity of the heterostructured OFETs by comparing responses upon exposure to different interference vapors with response to DMMP exposure. Much higher response was observed in the case of DMMP, even when the concentration of DMMP vapor was much lower than other analytes. Microstructures of OSC were characterized by scanning electron microscopy (SEM) and X-ray diffraction (XRD), revealing that the organic mixture has similar crystal structure and surface morphology to those of single component OSC films, indicating that the enhanced performance of the mixture is due to its chemical properties, rather than microstructural effects.

Introduction

Organic field-effect transistors (OFETs) are projected for application in circuits of moderate complexity, such as display drivers, radio frequency identification tags, or pressure mapping elements.[1−3] A compelling additional application of organic electronics is chemical sensing, especially of vapors. This is due to the ability to covalently attach receptors for compounds of interest to the molecules that make up the organic semiconductor (OSC), in locations where analyte−receptor binding will strongly influence the current flowing across a transistor channel. Responses are simply noted as changes in the output source drain current for a given set of input drain voltages and gate voltages as the vapor adsorbs onto the OFET.

Various OSCs including phthalocyanines and naphthalenetetracarboxylic dianhydride are sensitive to gases such as oxygen, nitrogen dioxide, ammonia, carbon monoxide, and hydrogen sulfide.[4,5] A virtual array of 11 different OSCs in OFETs showed distinguishable (0.8−0.3-fold reductions and 1.5−2-fold increases) responses for different classes of analytes, in the absence of any particular receptor for the analytes.[6] Analyte concentrations of 10−100 ppm in the vapor phase were detected. A second virtual array study has recently appeared.[7]

It was later found that devices that included grain boundaries were much more sensitive to pentanol vapor than were the single-crystal devices, indicating that grain boundaries were a main adsorption site in this class of film.[8] A following study was published reporting distinctions in the nonspecific responses of pentacene OFETs to pentanol depending on whether the devices were grain boundary or single-grain dominated,[9] consistent with the results of our preliminary study. Thus, the sensitivity of OFETs is highly correlated with topographic features in the films.

Some recent progress has been made using carbon nanotube sensing elements for vapors,[10,11] though rational vapor−receptor interactions were not utilized. Inorganic and nanostructured semiconductors are aimed at single-molecule detection but are not as well suited for large-area sensing. In some cases, the responses are irreversible and may be occurring at contacts rather than the semiconductors themselves.[12,13] Swellable polymers[14−18]

[†] Department of Materials Science and Engineering.
[‡] Applied Physics Laboratory.

(1) Kelley, T. W.; Baude, P. f.; Gerlach, C.; Ender, D. E.; Muyres, D.; Haase, M. A.; Vogel, D.; Theiss, S. D. *Chem. Mater.* **2004**, *16*, 4413−4422.
(2) Parashkov, R.; Becker, E.; Riedl, T.; Johannes, H. H.; Kowalsky, W. *Proc. IEEE* **2005**, *93*, 1321−1329.
(3) Someya, T.; Sekitani, T.; Iba, S.; Kato, Y.; Kawaguchi, H.; Sakurai, T. *Proc. Natl. Acad. Sci. U.S.A.* **2004**, *101* (27), 9966−9970.
(4) Guillaud, G.; Simon, J.; Germain, J. P. *Coord. Chem. Rev.* **1998**, *180*, 1433−1484.
(5) Torsi, L.; Dodabalapur, A.; Cioffi, N.; Sabbatini, L.; Zambonin, P. G. *Sens. Actuators, B* **2001**, *77* (1−2), 7−11.
(6) Crone, B.; Dodabalapur, A.; Gelperin, A.; Torsi, L.; Katz, H. E.; Lovinger, A. J.; Bao, Z. *Appl. Phys. Lett.* **2001**, *78* (15), 2229−2231.
(7) Liao, F.; Chen, C.; Subramanian, V. *Sens. Actuators, B* **2005**, *107*, (2), 849−855.
(8) Torsi, L.; Lovinger, A. J.; Crone, B.; Someya, T.; Dodabalapur, A.; Katz, H. E.; Gelperin, A. *J. Phys. Chem. B* **2002**, *106*, 12563−12568.
(9) Wang, L.; Fine, D.; Dodabalapur, A. *Appl. Phys. Lett.* **2004**, *85*, 6386−6388.
(10) Snow, E. S.; Perkins, F. K.; Houser, E. J.; Badescu, S. C.; Reinecke, T. L. *Science* **2005**, *307*, 1942−1945
(11) Staii, C.; Johnson, Alan T., Jr.; Chen, M.; Gelperin, A. *Nano Lett.* **2005**, *5* (9), 1774−1778.
(12) Ramanathan, K.; Bangar, M. A.; Yun, M.; Chen, W.; Myung, N. V.; Mulchandani, A. *J. Am. Chem. Soc.* **2005**, *127*, 496−497.

10.1021/ja068964z CCC: $37.00

Scheme 1

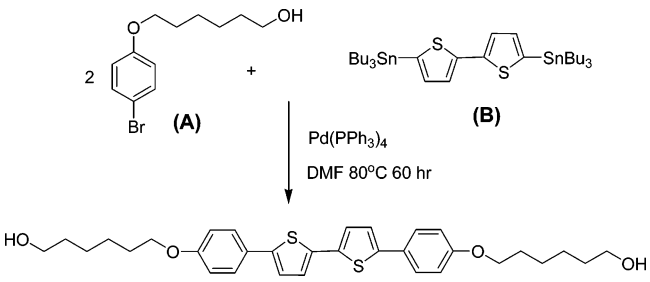

have been used to form arrays with specific responses but are limited by diffusion times within the polymers. Organic semiconductors offer the opportunity to employ much more facile deposition procedures and to covalently bind receptors for analytes of interest at highly accessible regions within tens of angstroms of the conductive path or "channel" in OFET terminology. The binding chemistry is much better defined than with inorganic semiconductors, and the binding position greatly increases response speed relative to thicker polymer devices. While OFET sensor work is ongoing at several institutions, OFETs have not yet been designed for optimal binding ability or film morphology for any particular analyte of interest, and not specifically for nerve agent simulants that are of urgent interest for security applications. The responses also have not been correlated with theoretical predictions about sensitivity and selectivity.

In this manuscript, we report initial studies of hole-transporting phenylene−thiophene tetramers, with and without hydroxyl functionalization, interacting with the weakly basic analyte dimethyl methylphosphonate (DMMP) that simulates phosphonate nerve agents. The hydroxy group is the simplest receptor that could be utilized for enhancing this interaction. We further demonstrate the use of two-layer and mixed tetramer films for the simultaneous optimization of sensitivity and response speed.

Experimental Section

Materials: The semiconductor 5,5′-bis(4-*n*-hexyl-phenyl)-2,2′-bithiophene (6PTTP6) was synthesized according to known procedures,[19] and 5,5′-bis(4-hydroxyhexyloxyphenyl)-2,2′-bithiophene (HO6OPT) was synthesized as shown in Scheme 1. To a solution of 15 g (82.8mmol) of 6-bromo-1-hexanol in 75 mL of DMF, 12.98 g (75 mmol) of 4-bromo-phenol were added, followed by the addition of 9 g (80.4 mmol) of potassium *tert*-butoxide. The reaction mixture was stirred overnight at 70 °C in N_2. After cooling to room temperature, the mixture was poured into 200 mL of ether and washed with aqueous NaOH (2%, 50 mL) and water (100 mL, 3 times). The organic layer was dried over $MgSO_4$ and evaporated in vacuo, yielding 15.5 g (56.7 mmol, 76%) of compound **A** as an oil. NMR ($CDCl_3$) δ 1.4−1.5 (4H), 1.6 (2H), 1.8 (2H), 3.66 (t, 2H), 3.92 (t, 2H), 6.77 and 7.35 (ABq, 4H).

The reagent **B** 5,5′-bis(tri-*n*-butylstannyl)-2,2′-bithiophene was synthesized as follows: 2.5 M *n*-BuLi in hexane (22 mL, 55mmol) was added dropwise to a solution of 2,2′-bithiophene (4.16 g, 25mmol) in 170 mL of THF at −78 °C with stirring in N_2. After a white precipitate formed, the mixture was warmed to room temperature and stirred for 1 h. Tri-*n*-butyltin chloride (14 mL, 52mmol) was added in the mixture, and then the mixture was heated to gentle reflux for 1 h. The solution was allowed to cool to room temperature, and then 400 mL of *n*-hexane were added to the solution. The organic layer was washed with aqueous Na_2CO_3 (5%, 125 mL) and water (125 mL twice). The organic layer was dried over $MgSO_4$ and evaporated in vacuo to give a dark brown product (17.8 g, 96%). NMR ($CDCl_3$) δ 0.91, 1,13, 1.36, 1.56 (Bu), 7.05, 7.29 (ABq, thiophene H).

The mixture of compound **A** (5.77 g, 21.2mmol), compound **B** 5,5′-bis(tri-*n*-butylstannyl)-2,2′-bithiophene (6.9 g, 9.3mmol), and $Pd(PPh_3)_4$ (0.5 g, 0.7mmol) in 100 mL of DMF was stirred for 60 h under N_2 at 80 °C. The dark brown precipitate was collected and washed with MeOH and toluene, yielding a dark brown product. The crude solid was hot-filtered and recrystallized with DMF to yield 0.94 g of yellow-brown solid. 0.6 g of the crude product was further purified by vacuum sublimation and gave 0.38 g pure yellow product. Mp 244−248. Mass Spectrum: 550 (M+), 350 (base peak). Anal. Calcd for $C_{32}H_{34}S_2O_4$: C, 69.78; H, 6.95; S, 11.6. Found: C, 68.99; H, 6.67; S, 12.2.

Analyte Compounds: 2-Octanone, butyl butyrate, acetic acid, dibutylamine, and DMMP were purchased from Aldrich, and diisopropyl methylphosphonate (DIMP) was purchased from Alfa Aesar. All of the compounds were used as received without further purification. Several tests were performed to verify the purity and authenticity of the DMMP. The pH value of the DMMP aqueous extract was found to be neutral, indicating the absence of basic impurities. GC−MS was also performed to check the purity of DMMP. With an *S*/*N* ratio of 100, the mass value of the major peak is 124, and no impurity was detected. Because GC−MS cannot detect highly volatile impurities, NMR measurement was performed additionally, and only a tiny peak centered at 3.44 ppm in the NMR spectrum can be considered as an impurity peak. The impurity peak was attributed to the CH_3 group of methanol. The peak height is less than 0.15% of DMMP OCH_3 peaks, suggesting that less than 0.15 mol % (<0.1 wt %) of methanol may be present, the upper limit of possible impurity concentration. Further checks for methanol interference were performed, as described in the Results and Discussion.

Device Fabrication: Figure 1 is the schematic illustration of the OFET "sensors". Heavily doped silicon wafers with 300 nm of thermally grown silicon dioxide served as substrates for all the devices. The silicon dioxide layers on the corner of all devices were scratched away to access the silicon as gate electrodes. Substrates were cleaned by 20 min sonication in acetone followed by rinsing with 2-propanol. Organic semiconductor thin films were deposited by vacuum evaporation at a pressure < 10^{-5} mbar. The substrate temperature was kept nominally at room temperature, rather than at elevated temperature, in order to maximize grain boundaries.[8,20] For the 6PTTP6 "device 1", 50 nm of 6PTTP6 thin film were deposited. For a "blend" device, we coevaporated the blend layers as follows: We used a thermal evaporator with two source boats, with 6PTTP6 in one boat and HO6OPT in the other one. The evaporation rates of each material were adjusted to be 1.2 Å/s before the shutter was opened. During evaporation, the total evaporation rate of the two materials varied in the range 2.4 to 2.8 Å/s. With this method, two semiconductor materials can be evaporated briefly at the same deposition rates. For the single layer blend (device 2), 6PTTP6 and HO6OPT were coevaporated and resulted in 50 nm of film. For the two-layer blend (device 3), 35 nm of 6PTTP6 film were evaporated, followed by the coevaporation of 15 nm of 6PTTP6 and

(13) Chen, R. J.; Choi, H. C.; Bangsaruntip, S.; Yenilmez, E.; Tang, X.; Wang, Q.; Chang, Y.-L.; Dai, H. J. *J. Am. Chem. Soc.* **2004**, *126*, 1563−1568.
(14) Lonergan, M. C.; Severin, E. J.; Doleman, B. J.; Beaber, S. A.; Grubb, R. H.; Lewis, N. S. *Chem. Mater.* **1996**, *8* (9), 2298−2312.
(15) Albert, K. J.; Lewis, N. S.; Schauer, C. L.; Sotzing, G. A.; Stitzel, S. E.; Vaid, T. P.; Walt, D. R. *Chem. Rev.* **2000**, *100* (7), 2595−2626.
(16) Gao, T.; Tillman, E. S.; Lewis, N. S. *Abstracts of Papers of the American Chemical Society* **2004**, *227*, U504.
(17) Gao, T.; Tillman, E. S.; Lewis, N. S. *Chem. Mater.* **2005**, *17* (11), 2904−2911.
(18) Gao, T.; Woodka, M. D.; Brunschwig, B. S.; Lewis, N. S. *Chem. Mater.* **2006**, *18* (22), 5193−5202.
(19) Mushrush, M.; Facchetti, A.; Lefenfeld, M.; Katz, H. E.; Marks, T. J. *J. Am. Chem. Soc.* **2003**, *125* (31), 9414−9423.
(20) Someya, T.; Katz, H. E.; Gelperin, A.; Lovinger, A. J.; Dodabalapur, A. *Appl. Phys. Lett.* **2002**, *81* (16), 3079−3081.
(21) Guillaud, G.; Simon, J.; Germain, J. P. *Coord. Chem. Rev.* **1998**, *178*−*180*, 1433−1484.
(22) Horowitz, Gilles; Hajlaoui, M. E. *Adv. Mater.* **2000**, *12* (14), 1046−1050.

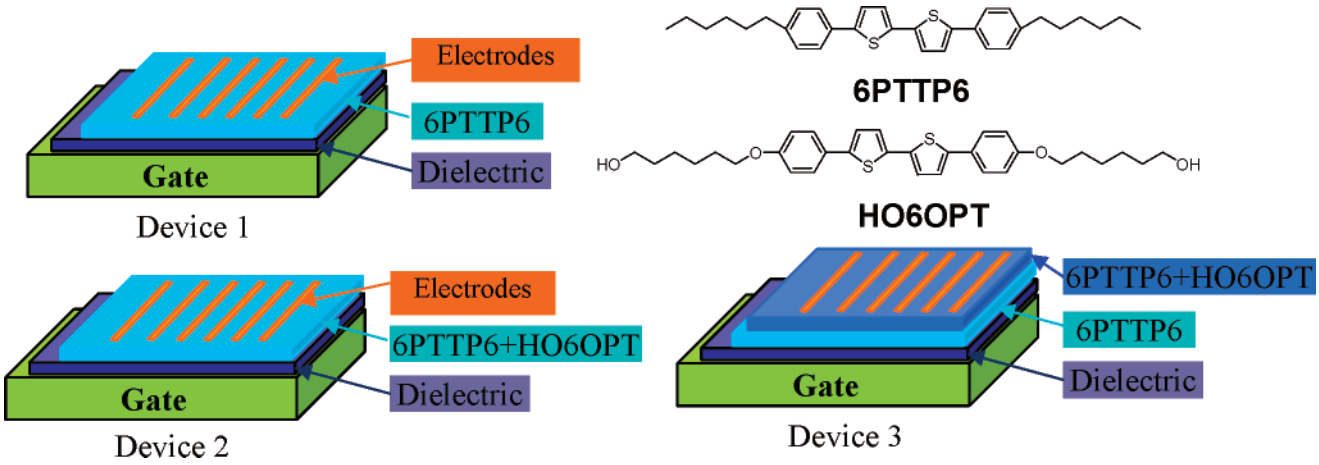

Figure 1. Schematic illustration of OFETs and semiconductor molecular structures: device 1, 6PTTP6; device 2, single-layer blend; device 3, two-layer blend.

HO6OPT unless otherwise specified. Top-contact source and drain electrodes were fabricated by thermal evaporation of gold through a shadow mask with a spacing of $L = 270$ μm and $W = 6.5$ mm.

Measurement: As p-channel transistors, all the current−voltage ($I-V$) curves of the devices were measured in the accumulation mode. While the source was set to be common, the source−drain (V_d) was swept between 0 and −80 V, the gate voltage was stepped from −20 V to −100 V with a −20 V step size unless described specifically, and the saturation source−drain currents were recorded as the output signals of sensors. We did not start with zero gate voltage when we tested the sensor performance, because the source−drain current is too small and the sensor performance is not very stable with $V_g = 0$.

The sensors were tested in a 1 ft^3 (28 L) chamber. For the measurement of the sensor performance in DMMP vapor with concentration varying over time, the chamber was initially filled with air, and then a vial containing liquid DMMP was placed into the closed chamber. The initial evaporation rate of DMMP was obtained by determining the mass loss of the DMMP before and after the vial containing DMMP liquid was kept in an open space for unit time. At room temperature, the evaporation speed was measured to be 2.325 μmol/min, corresponding to a 1.8 ppm/min molar concentration change in the 1 ft^3 chamber. At room temperature, the saturation vapor concentration of DMMP is 1620 ppm (mol/mol) at 21 °C.[23] After an hour of evaporation from the vial, the concentration of DMMP vapor in the chamber should be no more than 60 × 1.8 = 108 ppm (<7% of the saturation concentration of DMMP vapor), considering the adsorption of DMMP on the chamber wall, and the decreasing evaporation speed of DMMP due to the decreasing vapor pressure gradient between the liquid surface and vapor phase in the chamber with time. Within 1 h, we can roughly consider the evaporation speed of DMMP to be constant at 1.8 ppm/min and the DMMP vapor concentration to be increasing linearly in the test chamber, since the change of the vapor pressure gradient between the liquid surface and vapor phase in the chamber is small.

For measurement at relatively constant analyte vapor concentration, the test chamber was connected to a constant flow rate of gas, which was switched between N_2 and analyte vapors. Bubblers containing analyte liquids were used as sources of analyte vapors. N_2 gas flowed above the liquid surface and delivered certain amounts of analyte vapor to the test chamber. The mass of the bubblers was measured before and after testing to determine the total mass of analyte delivered by a specific volume of carrier gas and, thereby, calculate the average concentration of analyte vapors in the test chamber. The sensors were placed far away from the outlet of the analyte vapor to avoid direct flush, so that the analyte vapors were delivered gently to the sample, except as noted later. The setup was calibrated using a handheld chemical detector (ProEngin, model: AP4C), which analyzes for phosphorus atoms in gas-phase molecules using flame photometric detection. The dynamic range of the AP4C is 24 ppb ≈ 13 ppm of DMMP. We generated diluted DMMP vapor by mixing an N_2 stream with N_2 blown over a DMMP source and measured the DMMP concentration with the AP4C. The DMMP concentration of the vapor generated by our setup was calculated by the rates of mass loss in bubblers and gas flow into the chamber to be 7.3 ppm, while 7.02 ppm was the reading obtained using the AP4C. During our device tests, 150 and 20 ppm DMMP vapors were generated by the same dilution method.

Where devices were exposed to air, the relative humidity was 20−40% and did not change materially during the course of any experiment.

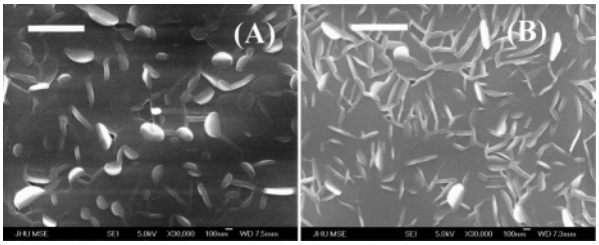

Figure 2. Scanning electron microscopic imagines of organic semiconductor films: (A) 6PTTP6; (B) blend of HO6OPT and 6PTTP6. Scale bars denote 1 μm.

Results and Discussion

Microstructure Characterization: Various factors such as film composition, OSC molecular structures, degrees of crystallinity, surface morphologies, and grain boundaries can influence the sensing performance of organic thin films.[21] We investigated the microstructures of the organic semiconductor films in order to understand if the variations in the performance of devices are due to the film compositions or differences in film microstructures.

Figure 2 shows the scanning electron microscopic images (JEOL 6700F) of the pure 6PTTP6 film and the two-layer blend of HO6OPT-6PTTP6 evaporated on SiO_2/Si substrates at room temperature. Both films show platelike structures, with the topmost layer of plates partially standing perpendicular to the surfaces. For the sensor application, surface structures like these films are desired because of their larger surface area and more adsorption sites compared to films with large bulk grains. The densities of the upright plates of two films are different, but

(23) Kyle, C.; Kulkarni, R. D.; Kozlov, M.; Manohar, S. K. *Nanotechnology* **2006**, *17*, 4123−4128.

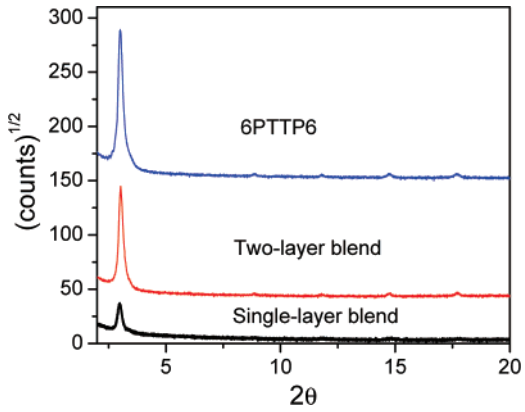

Figure 3. X-ray diffraction patterns of the pure 6PTTP6 film, single-layer blend film, and two-layer blend film.

both films are organized similarly by very thin layers stacking together, which is a typical structure for oligomer semiconductors.[22]

X-ray diffraction measurements (Philips X Pert Pro) were performed along the surface normal axis for all devices to understand the degree of crystallization of the semiconductor films. As shown in Figure 3, the pure 6PTTP6 film (device 1), single layer blend film (device 2), and two-layer blend film (device 3) exhibit essentially identical XRD patterns and d-spacings, indicating the high similarity of the crystallinities between pure 6PTTP6 and the blend films.

Current Voltage Characteristics of OFET Sensors: The I_d-V_d characteristics of all three OFET sensors are shown in Figure 4. All of the three OEFT sensors exhibited obvious linear and saturation regions and showed negligible gate leakage current at $V_d = 0$. The maximum leakage current for a two-layer blend was 2 nA, at least 3 orders of magnitude lower than the typical output currents. For most of the sweep, the leakage current is a few tenths of a nA, of similar order as the charging current: 10^{-8} F/cm^2 oxide capacitance times 0.015 cm^2 channel area times 10 V/s gate sweep rate. The mobility of the single-layer blend OFET is apparently much lower than that of 6PTTP6 and two-layer blend OFETs.

Performance of Nonfunctionalized Devices: 5,5′-Bis(4-*n*-hexyl-phenyl)-2,2′-bithiophene (6PTTP6) Field Effect Transistor. The nonfunctionalized 6PTTP6 film is inherently sensitive to DMMP. Figure 5a shows the response of the saturation source−drain current of a 6PTTP6 OFET (device 1) as a function of time at various gate voltages during DMMP exposure. Device 1 was tested in a chamber filled with air. The black solid line indicates the time when a vial with DMMP liquid was placed into the closed chamber. The saturation source−drain current I_d decreased significantly during exposure to DMMP. We also observed that the current drifts have an obvious gate voltage dependence. In Figure 5b, saturation source−drain currents with different gate voltages were normalized by the value at time = 0 min and plotted as a function of time. The saturation source−drain current reduced to less than 5% of its original value with the gate voltage set to −20 V, corresponding to a large relative response, while it only reduced to around 30% with V_g set to −100 V.

The saturation source−drain current of this unfunctionalized sensor reached the minimum value after 40 min of exposure to DMMP vapor, during which time the DMMP concentration in the chamber was considered to have increased linearly to 75 ppm. The kinetics of the response are controlled by the evaporation rate of DMMP and slow diffusion rate of DMMP within the OSC film.[24,25] The adsorption of DMMP molecules on the unfunctionalized semiconductor organic film surface is probably a weak electrostatic force of the van der Waals type.[26]

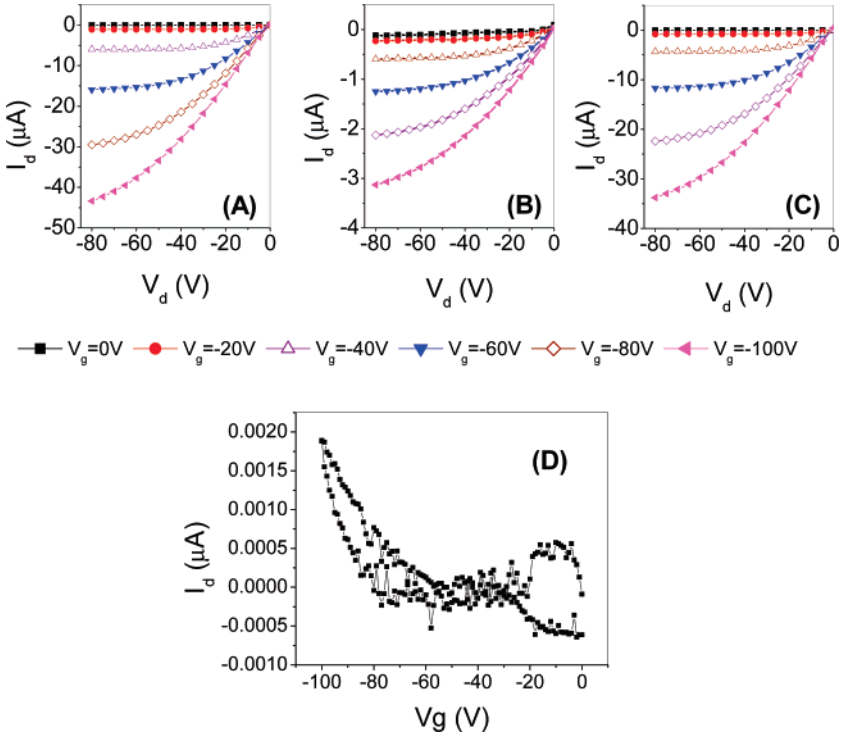

Figure 4. I_d-V_d characteristics of (A) 6PTTP6 OFET; (B) Single-layer blend OFET; (C) Two-layer blend OFET. Also, (D) leakage current for two-layer blend with source and drain grounded and gate swept from 0 to −100 V.

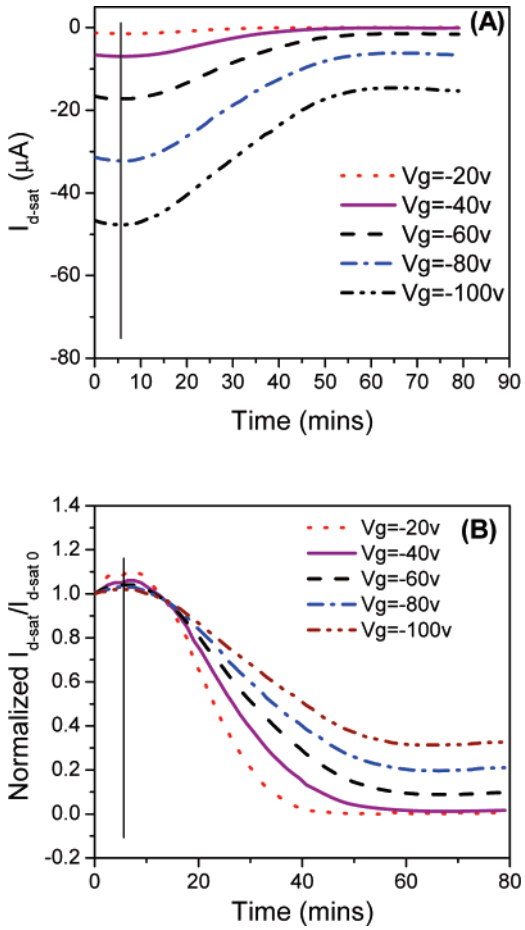

Figure 5. Responses of the saturation drain current of 6PTTP6 sensor as a function of time at various gate voltages during DMMP exposure. The black solid vertical line indicates the time when the device was exposed to DMMP: (A) saturation source−drain current; (B) relative response: $I_{d-sat}/I_{d-sat\ 0}$.

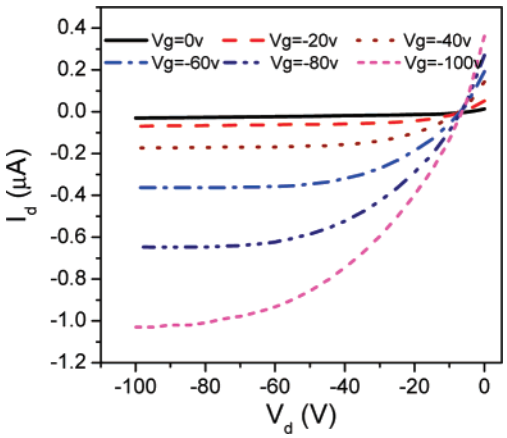

Figure 6. Drain current I_d vs drain voltage V_d curves at various gate voltage V_g of a HO6OPT field-effect transistor.

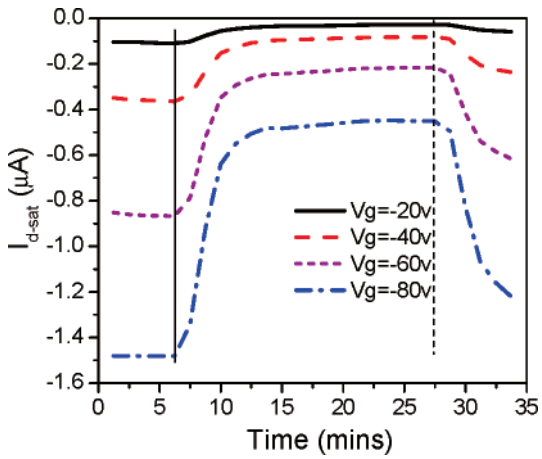

Figure 7. Response of the single-layer blend on exposure to DMMP vapor. The black solid vertical line indicates the time when a vial with DMMP liquid was placed into the closed chamber, and the dash vertical line indicates the time when the vial was removed and the chamber was open to air.

Performance of Functionalized Devices: Organic Sensors Based on Blends of HO6OPT and 6PTTP6. In order to enhance the sensitivity and response speed of the sensor, we synthesized a functionalized organic semiconductor material, 5,5′-bis(4-hydroxyhexyloxyphenyl)-2,2′-bithiophene (HO6OPT), as receptor material. HO6OPT has a similar molecular structure to 6PTTP6; however it has OH groups on the end of the molecule. The OH group should form hydrogen bonds with DMMP, leading to increased adsorption and electronic effects.

Figure 6 shows the typical I_d-V_d curve of a field effect transistor with HO6OPT as an active layer. The gate leakage current was due to the use of a large substrate without gate-electrode patterning. The field effect mobility of this device is much lower and less precisely determined than that of 6PTTP6, but it verified the semiconductor activity of the HO6OPT compound. For the sensor application, it is more desirable to have a higher current, so that the HO6OPT FET was not optimized further and not employed as a sensor.

Instead of the single component HO6OPT FET, we developed a heterostructure (device 3; Figure 1), within which there are two layers of organic semiconductors on the substrate: the bottom layer is 35 nm of 6PTTP6 serving as charge transport layer, and the top layer is 15 nm of the blend of two materials, HO6OPT and 6PTTP6, which can provide a moderate distribution of OH groups as receptor sites. In order to better understand this blend structure, we also fabricated the single layer blend field effect transistor (device 2: Figure 1), which has a 50 nm single layer of the blend of HO6OPT and 6PTTP6 as the active layer.

As shown in Figure 4b, the single-layer blend OFET exhibited good linear and saturation regions. Figure 7 represents the response of the single layer blend (device 2) on exposure to DMMP vapor in air under ambient conditions. The DMMP vapor was again generated by placing the vial containing DMMP liquid into the test chamber. The sensing measurements have clearly indicated that the sensor with the blend film has a shorter response time than that of the 6PTTP6 OFET. The saturation source−drain current of this functionalized sensor decreased dramatically right after the vial was placed into the chamber, and it reached the minimum value after about 10 min of exposure to DMMP vapor. The saturation current of this device compared to device 1 is still 1 order of magnitude lower, which is a disadvantage for the sensor application. We therefore employed the two-layer blend structure of device 3.

The sensing response of the two-layer blend device 3 to DMMP vapor in air under ambient conditions is shown in Figure

(24) Zimmermann, C.; Rebière, D.; Déjous, C.; Pistré, J.; Chastaing, E.; Planade, R. *Sens. Actuators, B* **2001**, *76*, 86−94.
(25) Zhou, R.; Josse, F.; Göpel, W.; Öztürk, Z. Z.; Bekaroğlu, Ö. *Appl. Organomet. Chem.* **1996**, *10* (8), 557−577.
(26) Bouvet, M. *Anal. Bioanal. Chem.* **2006**, *384*, 366−373.

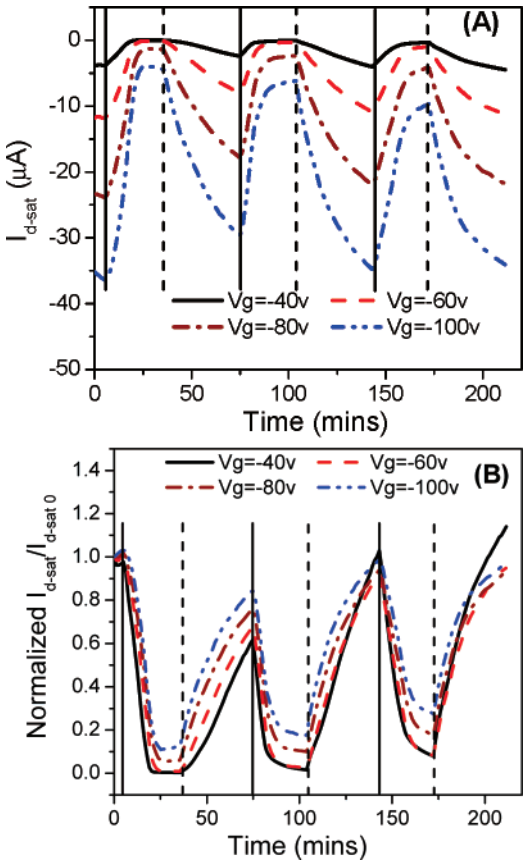

Figure 8. Sensing response of the two-layer blend sensor to DMMP vapor. The black solid vertical line indicates the time when a vial with DMMP liquid was placed into the closed chamber, and the dash vertical line indicates the time when the vial was removed and the chamber was open to air. (A) The saturation source−drain current versus time; (B) the relative response of the drain current versus time.

8 for various gate voltages. Again, the black solid vertical line indicates the time when a vial with DMMP liquid was placed into the closed chamber filled with air, while the dashed vertical line shows the time we remove the vial and open the chamber to air. We cycled these 3 times to show both the response and subsequent recovery of the current. The absolute current is 1 order of magnitude higher than that of device 2, while the variation of the saturation source−drain current versus time was found to be similar to that for the single layer blend sensor (device 2). The high current can be attributed to the bottom layer of the high mobility semiconductor: 6PTTP6, which provides charge transport. Studies[27,28] have shown that, in the accumulation regime of evaporated oligomer film, most mobile charge carriers (more than 80% at high gate voltage)[29] are concentrated within the first two semiconductor monolayers at the dielectric−semiconductor interface. XRD shows that the monolayer spacing of 6PTTP6 is 3 nm, suggesting that the effective thickness of conducting channel is around 6 nm for this type of transistor. The film thickness of the bottom 6PTTP6 layer of this device is 35 nm, which is much thicker than the effective thickness of the conducting channel. As a result, the top blend layer should not practically influence the charge

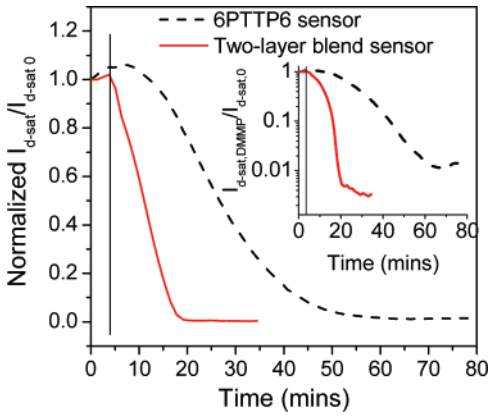

Figure 9. Sensing responses of the two-layer blend and 6PTTP6 itself to DMMP vapor generated by a vial containing DMMP liquid. The inset shows the log plot of the same curves.

transport along the conducting channel, and the saturation source−drain current of this two-layer blend should be comparable to that of device 1. Therefore, the response of the heterostructure is probably due to the trapping or hindering of charge carriers digressing from the channel or from a small amount of the top layer that penetrates to the channel between grains, where DMMP adsorbs.

Figure 9 compares the responses of the ratio of the normalized saturation source−drain current I_d/I_{d0} of device 1 and device 3 as a function of time during DMMP exposure, with V_g set to be −40 V. The blank vertical line indicates the time when a vial with DMMP liquid was placed into the closed chamber. Comparing the two plots in Figure 9, we observed that device 3 has a much stronger and faster response than that from device 1 especially during the first period of the evaporation of DMMP vapor from the vial, when the concentration of DMMP vapor is presumably low.

Figure 10a shows the two-layer blend sensor responses to 150 ppm DMMP vapor. We vent the chamber with N_2 and then delivered 150 ppm DMMP with N_2 for 6 min. The shadowed areas in the plot indicate when the DMMP vapor is flowing above the sensor. The sensor was heated at 45 °C for 2 min in air and cooled down in N_2 before test. The saturation drain current decreased significantly when the DMMP vapor was injected into the chamber. The observed response times are comparable to many for reported sensors.[10,30,31]

In practical a sensing operation, heating the sensor at 45 °C for 2 min is sufficient to fully recover the sensor. Figure 10 shows the reproducible responses and recovery of two-layer blend sensors upon exposure to 150 ppm DMMP vapor. The sensor was heated at 45 °C for 2 min in air and cooled down in N_2 between every measurement. Figure 10b was obtained from a fresh two-layer blend FET, while Figure 10c shows the response of a used sensor that has been tested many times previously. The two sensors exhibited similar responses. The same sensing tests were also performed with other two-layer blend OFETs fabricated 6 months earlier, and similar results were obtained.

(27) Horowitz, G.; Hajlaoui, R.; Bourguiga, R.; Hajlaoui, M. *Synth. Met.* **1999**, *101*, 401−404.
(28) Horowitz, G. *J. Mater. Res.* **2004**, *19* (7), 1946−1962.
(29) Horowitz, G. Organic Transistors. In *Organic Electronics*; Klauk, H., Ed.; Wiley-VCH: Weinheim, Germany, 2006; pp 3−32.
(30) Tomchenko, A. A.; Harmer, G. P.; Marquis, B. T. *Sens. Actuators, B* **2005**, *108*, 41−55.
(31) Patel, S. V.; Mlsna, T. E.; Fruhberger, B.; Klaassen, E.; Cemalovic, S.; Baselt, D. R. *Sens. Actuators, B* **2003**, *96*, 541−553.

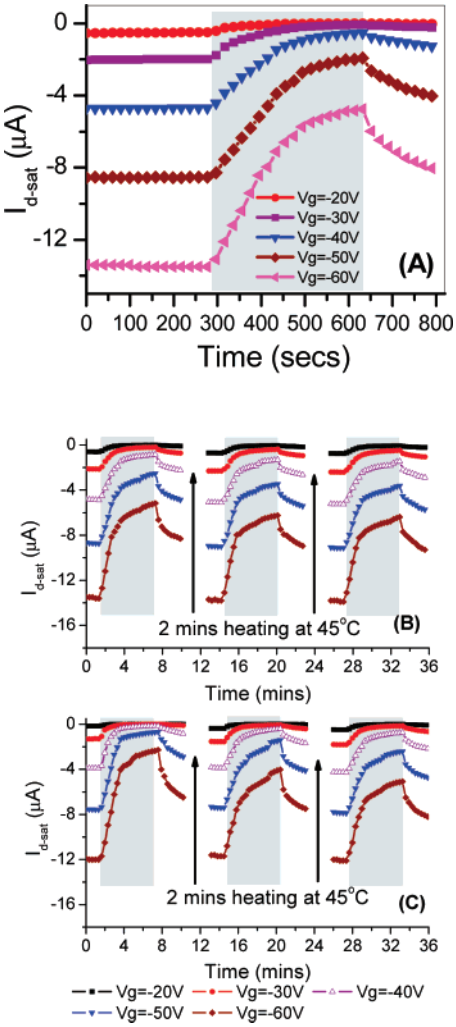

Figure 10. Reversible responses of two-layer blend films upon exposure to 150 ppm DMMP vapor. (A) Device preheated; (B) fresh device; (C) used device.

We checked to see if the response times were determined by convection through the large sample chamber or by diffusion through the thickness of the two-layer film. Figure 11a shows the response of 35 nm of 6PTTP6 with 15 nm of the blend on top of 150 ppm DMMP, delivered through a hose located about 1 cm from the device surface. The time scale is similar to that observed in Figure 10. On the other hand, the response speed is much faster for a thinner bilayer. Figure 11b shows the response of 6 nm of 6PTTP6 with 3 nm of the bilayer on top under the same conditions. The time scale has decreased by an order of magnitude. Thus, the response time is limited in the thick devices by the time for vapor molecules to diffuse to the positions where they have the maximum electronic effect. The use of thin devices should result in adequate response times for application. The maximum gate leakage current for the thin device was 0.06 nA.

From the same experiment shown in the middle curve of Figure 10b, field effect mobility μ_{sat} and threshold voltage V_t were extracted as shown in Figure 12. The shadowed area indicates the time when DMMP vapor was delivered. When the transistors are exposed to DMMP vapors, the change of saturation drain current can be attributed to the variation of both field effect mobility μ_{sat} and threshold voltage V_t. Hence the

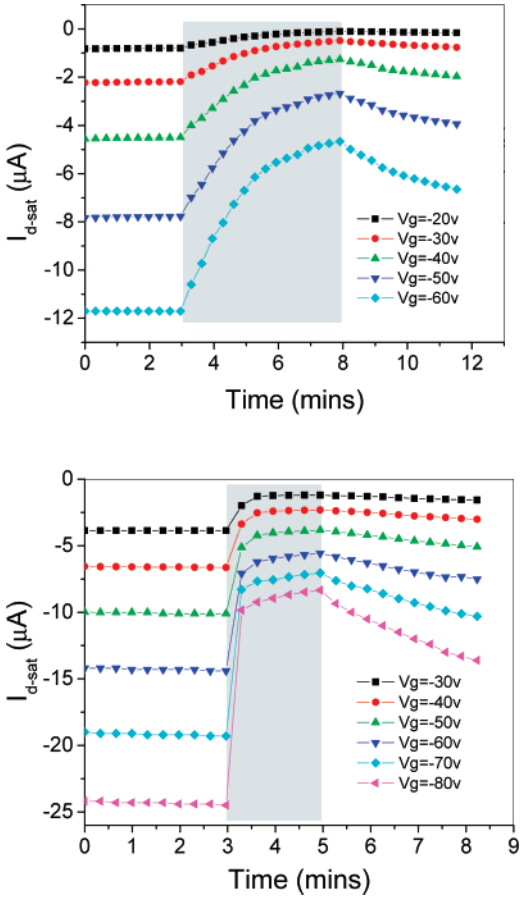

Figure 11. Absolute current response of "thick" (top) and "thin" (bottom) bilayer devices to 150 ppm of DMMP delivered via a hose 1 cm from the device surface beginning at the left edge of the gray region of the plot.

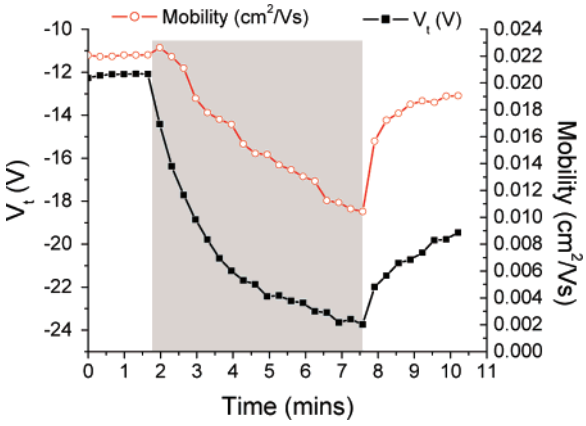

Figure 12. Mobility and threshold voltage response to DMMP vapor.

field effect mobility μ_{sat} and threshold voltage V_t can also be used as output signals of OFET sensors.

In order to verify that the change of the drain current of the two-layer blend sensor mainly resulted from DMMP, not from the possible trace methanol impurity, we also did two control experiments: A mixture of 1% of methanol and 99% of DMMP and a DMMP liquid sample that had been bubbled with N_2 for 30 min to remove possible volatile impurities were each used as analyte sources. The responses of the two-layer blend sensor to these two analytes were observed to be similar to that of fresh DMMP, suggesting that the responses of the sensor we observed are actually resulting from DMMP vapor.

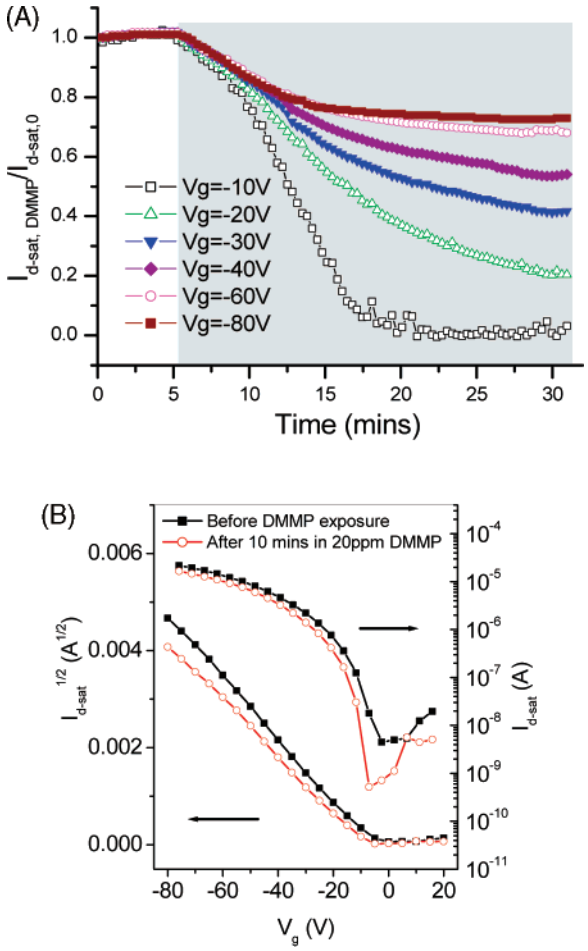

Figure 13. Two-layer blend response to 20 ppm DMMP vapor. (A) $I_{d-sat}/I_{d-sat,0}$ versus time. The shadowed areas indicate the time when the DMMP vapor is flowing above the sensor; (B) the saturation drain current before and after 10 min exposure to DMMP.

We have also obtained preliminary results of sensing DMMP vapor on the scale of 20 ppm. This time, the bubbler containing DMMP liquid was used as the source of DMMP vapor. N_2 gas flowed above the liquid surface at the rate of 4 L/min and delivered certain amounts of analyte vapor to a flask. The DMMP vapor was then further diluted by mixing with N_2 flowing into the flask at a rate of 28 L/min. The combined gases were directed into the test chamber. The mass of the bubbler was measured before and after testing, showing that the average concentration of DMMP vapors in the test chamber was 20 ppm. The two-layer film of 35 nm 6PTTP6 with 15 nm of the blend on top was preheated at 45 °C for 2 min followed by 2 min of cooling in N_2. The device was then tested in the 1 ft^3 chamber and showed an obvious response, though not as strong as that shown for higher concentrations at analogous voltages in Figures 8 and 10. As shown in Figure 13a, the drain current kept decreasing during the exposure time. In a second experiment, the drain voltage was fixed at −80V, and the gate voltage was swept from 20 to −80 V, with a −20 V step size. Figure 13b compares the saturation drain current of the device before and after 10 min of exposure to the 20 ppm DMMP vapor. The result suggests that sub-ppm sensing is achievable, though rates may be limited by diffusion through the films.[31,32]

Selectivity is a critical issue for chemical sensors. We investigated responses of the two-layer blend to a set of potential

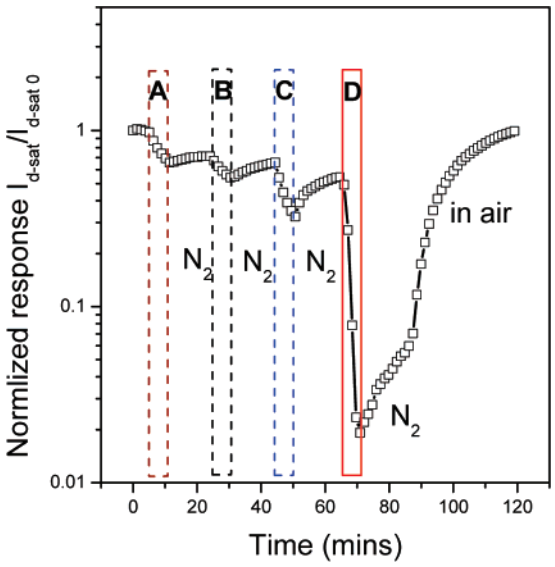

Figure 14. Response of the two-layer blend sensor to different analyte vapors: (A) 200 ppm 2-octanone; (B) 400 ppm butyl butyrate; (C) 5500 ppm acetic acid; (D) 150 ppm DMMP.

interference analytes with similar polarities or vapor pressures as those of DMMP and compared responses to that of DMMP vapor. 2-Octanone, butyl butyrate, and acetic acid were chosen to represent different groups of potential interference compounds containing double bonded oxygen atoms. Figure 14 shows the responses of the sensor to different analytes. The natural logarithm of the ratio of normalized drain currents $\ln(I_d/I_{d0})$ was potted versus time. The shadowed areas indicate when the sensor was exposed to 200 ppm 2-octanone, 400 ppm butyl butyrate, 5500 ppm acetic acid, and 150 ppm DMMP, respectively. We used higher concentrations of interference analytes than that of DMMP, to make the most conservative judgments about selectivity. The response of the two-layer blend sensor to DMMP is clearly much stronger than that to other interference vapors.

The responses of the two-layer blend sensor to dibutylamine (a secondary amine shaped like some mustard gases but somewhat more basic) and to 110 ppm of diisopropyl methylphosphonate (DIMP) were also studied with the same setup. As shown in Figure 15, the sensor exhibited a similar response to DIMP as that to DMMP vapor, suggesting that the sensor is sensitive to phosphonate compounds in general, not only to DMMP.

When dibutylamine was delivered into the test chamber, the OFET sensor was irreversibly quenched. In the practical application of sensors for weak bases, strongly basic interferents like amines will need to be filtered out in the sensor front end to avoid permanent quenching of the sensor.

Finally, we tested the same kind of two-layer device for humidity responses. Figure 16 shows the change in current as the relative humidity of air in the chamber is raised from 33 to 55%. The change is linear and considerably lower in magnitude than changes in response to DMMP. As a practical matter, any environmental sensor would be corrected for humidity effects by the use of membranes to filter water vapor at the front end,

(32) Ballantine, D. S.; White, R. M.; Martin, S. J.; Ricco, A. J.; Frye, G. C.; Zellers, E. T.; Wohltjen, H. *Acoustic Wave Sensors: Theory, Design and Physicochemical Application*; Academic Press: Boston, MA, 1997; Chapters 4 and 6.

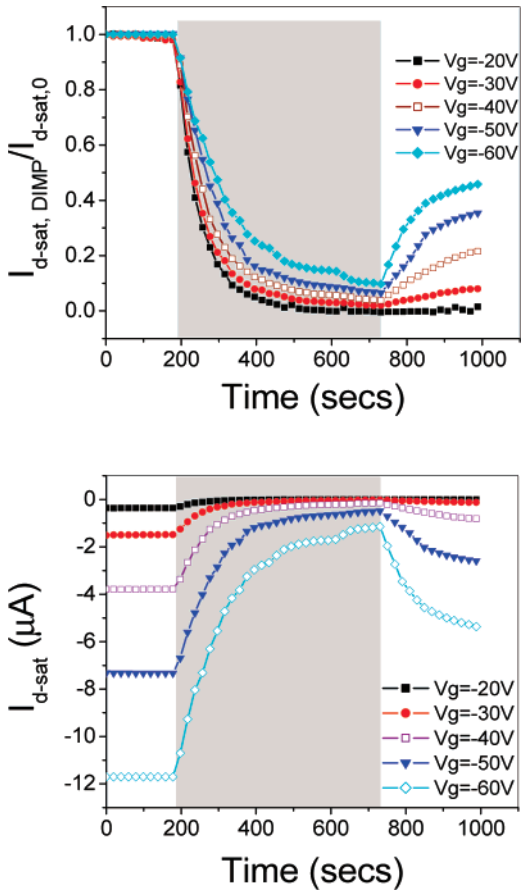

Figure 15. Two-layer blend FET response to 110 ppm DIMP.

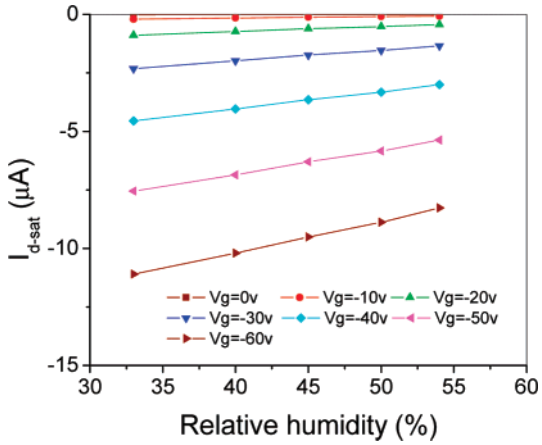

Figure 16. Current as a function of relative humidity for the bilayer device, with drain voltage held at −80 V. The experiment was performed over the course of 0.5 h.

and/or by employing a separate sensor to track humidity separately and correct the primary sensor for humidity effects. Even more likely, a larger sensor array would be employed to produce a specific response pattern to an analyte of interest.

Sensing Mechanism: The responses of the OFET based sensors are consistent with electrostatic modeling that we have done.[33] Figure 17a shows a schematic diagram of an OFET based chemical sensor and adsorbing DMMP molecules. E(g), the transverse source-gate field used to induce mobile charges,

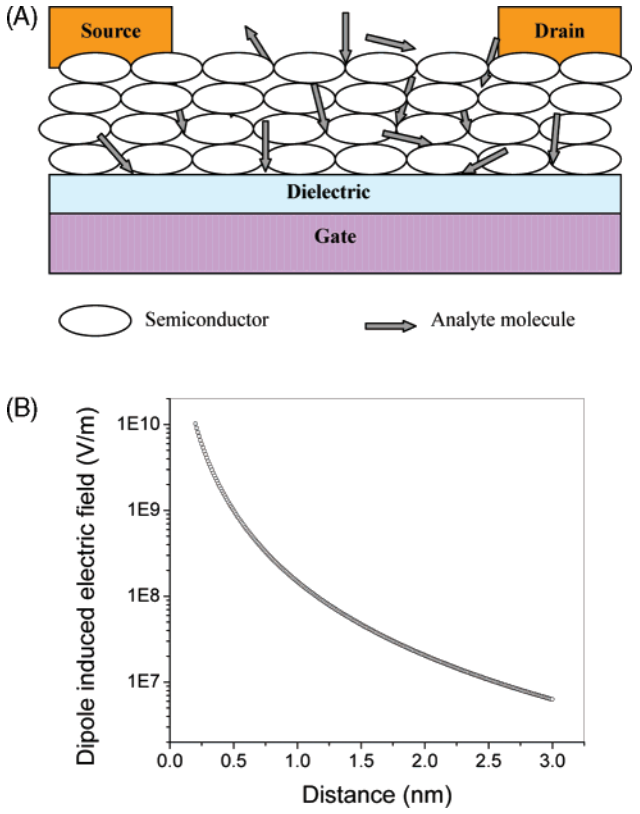

Figure 17. (A) A schematic diagram of an OFET based chemical sensor. (B) Dipole induced electric field at various distances in the direction parallel to the direction of the dipole moment.

is on the order of 10^8 V/m, and the longitudinal source−drain field E(SD) used to drive current through the channel is on the order of 10^6 V/m, with our device configuration. The DMMP molecule has a highly polarized P═O bond. Previous studies reported that the DMMP molecule has a dipole moment μ = 3−3.62 D, depending on the method of estimation and the conformation of the molecule.[10,34] In this paper, we use $\mu = 3$ D to get a conservative estimate of the dipole effect between DMMP and sensors.

The adsorption and diffusion of DMMP molecules into the semiconductor layer can induce strong electric fields in the immediate vicinity of the molecules (not in the entire channel!), which not only cause a portion of the mobile charges to be trapped and lose their activity but also effectively slow down the movement of charges that are still transported.[35] This action is probably mostly at the channel, resulting from vapor molecules diffusing amid the grains to approach the dielectric interface, or otherwise away from the channel, where charge carriers have a small but finite probability of drifting, both cases illustrated in Figure 17a.

The electric field induced by a dipole with a dipole moment of $\vec{p}$ can be calculated by the equation

$$\vec{E} = \frac{3K\,\vec{r}\,(\vec{p}\cdot\vec{r})}{r^5} - \frac{K\,\vec{p}}{r^3}$$

Here $K = 9 \times 10^9$ N·m^2/C^2 (Coulomb's constant), and $\vec{r}$ is the distance between the dipole and the position of concern.

(33) Katz, H. E.; Huang, J. Organic Semiconductor-based Chemical Sensors. In *Organic Electronics*; Klauk, H., Ed.; Wiley-VCH: Weinheim, Germany, 2006; pp 411−421.

(34) Vishnyakov, A.; Neimark, A. V. *J. Phys. Chem. A* **2004**, *108*, 1435−1439.

(35) Tanese, M. C.; Fine, D.; Dodabalapur, A.; Torsi, L. *Biosens. Bioelectron.* **2005**, *21*, 782−788.

Figure 17b plots the electric fields induced by a DMMP molecule in the direction parallel to the dipole moment as a function of the distance between DMMP and the position of concern. We noticed that the magnitude of the dipole induced field is comparable to E(g) and is much larger than E(SD), which means the dipoles of DMMP molecules are certainly capable of trapping mobile charges and significantly diminishing OFET current by changing both the threshold voltage V_t and the field effective mobility μ_{sat}.

Under the idealized assumptions including mobility independent of gate voltage and gradual channel approximation ((E(g) $\gg$ E(SD) in the present case), the saturation drain current I_{sat} of the device is given by eq 1[36]

$$I_{sat}^{1/2} = \left[\frac{W}{2L} C\mu_{sat}\right]^{1/2}(V_g - V_t) \quad (1)$$

When DMMP molecules are attached to semiconductors, dipoles induce changes in μ_{sat} and V_t, noted as $\Delta\mu$ and ΔV_t, so that the saturation drain current $I_{sat(DMMP)}$ of the device with DMMP becomes eq 2:

$$I_{sat(DMMP)}^{1/2} = \left[\frac{W}{2L} C(\mu_{sat} + \Delta\mu)\right]^{1/2}[V_g - (V_t + \Delta V_t)] \quad (2)$$

Combining eqs 1 and 2, we can get the relationship between $I_{sat(DMMP)}$ and I_{sat}, shown as eq 3:

$$I_{sat(DMMP)}/I_{sat} = \left(1 + \frac{\Delta\mu}{\mu_{sat}}\right)\left[1 - \left(\frac{\Delta V_t}{V_g - V_t}\right)\right]^2 \quad (3)$$

This equation is only valid when $|\Delta V_t| < |V_g - V_t|$, but it expresses the gate voltage dependence of the sensor responses. The value of V_g, V_t, and ΔV_t are all negative. For smaller values of $|V_g|$, such as 40 V, the $[1 - \Delta V_t/(V_g - V_t)]$ term is smaller, which results in a smaller value of the ratio of the saturation source−drain currents $I_{sat(DMMP)}/I_{sat0}$, corresponding to a more noticeable sensor response. On the contrary, if $|V_g|$ is larger, such as 100 V, the term $[1 - \Delta V_t/(V_g - V_t)]$ is larger than that of the previous case, which results in a relatively larger value of $I_{sat(DMMP)}/I_{sat0}$ and a smaller sensor response.

Figure 18a plots the square root of the saturation drain current of a 6PTTP6 FET versus gate voltages before and during DMMP vapor exposure. This time, V_d was set to be −100 V and V_g was swept from 20 to −100 V, with a −5 V step size. We can see that at lower $|V_g|$, the current ratio is larger. We can calculate the field effect mobility μ and threshold voltage V_t of the device before and after exposure to DMMP vapor by the slope of the curves and the intersection of the linear fitted curves with the X axis, as shown in Table 1. In Figure 18b, the closed squares correspond to the ratio of the saturation source−drain current $I_{sat(DMMP)}/I_{sat0}$ obtained from experiment. We performed a least-squares fit of those data, together with μ and V_t obtained from Figure 18a, to eq 3, which gives us an estimate of the value of ΔV_t and $\Delta\mu$. The estimated $\Delta V_t = -15.3$ V and the estimated $\Delta\mu = -0.0283$ cm^2/VS are very close to the values we obtained from experimental data, −16 V and −0.0277 cm^2/VS, respectively. This estimation is qualitative since the field effect mobility μ is actually also a function of V_g, and therefore the dependence of μ on V_g also contributes to the gate voltage dependence of the sensor responses. At high $|V_g|$ and $|V_d|$, the field effect mobility tends to saturate, and its gate voltage dependence is not that significant. However, at low gate voltage, μ increases linearly with V_g,[36] which explains the inconsistency between the experimental data and the fitted curve when $|V_g|$ is less than 25 V. When $|V_g|$ is larger than 90 V, the contact resistances cause much of the inconsistency between experimental and estimated data. Equation 3 is thus useful for estimating the voltage range over which a single sensing mechanism applies, and also for predicting responses at voltages not specifically included in a particular experimental dataset.

(36) Horowitz, G.; Hajlaoui, M. E.; Hajlaoui, R. *J. Appl. Phys.* **2000**, *87* (9), 4456−4463.

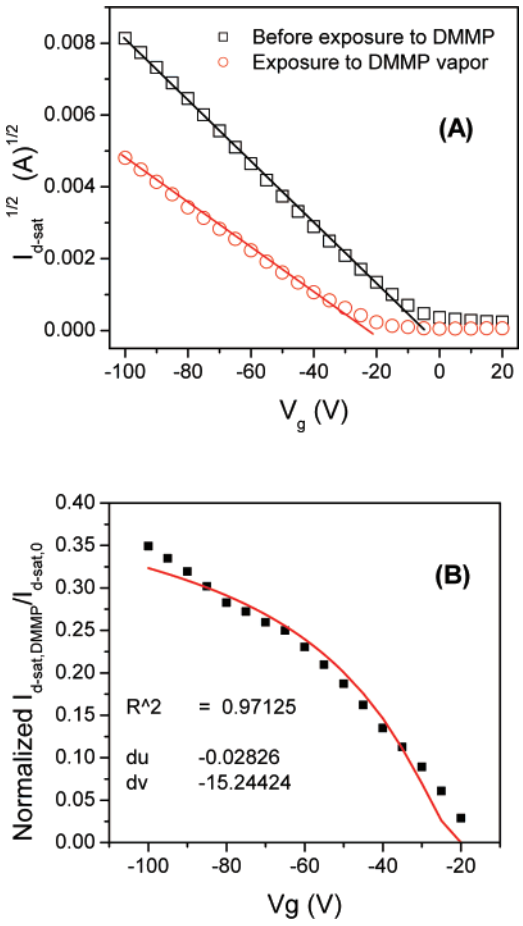

Figure 18. (A) Square root of the saturation drain current of a 6PTTP6 FET versus gate voltage before and during DMMP vapor exposure. (B) The closed squares correspond to the ratio of saturation source−drain current $I_{sat(DMMP)}/I_{sat0}$ obtained from experiment; the solid line is the least-squares fitted curve according to eq 3.

Table 1. Field-Effect Mobility μ_{sat} and Threshold Voltage V_t of 6PTTP6 FET before and after Exposure to DMMP Vapor

	V_t (V)	μ_{sat} (cm^2/V·s)	ΔV_t (V)	$\Delta\mu$ (cm^2/V·s)
no DMMP	−5	0.0522	−16	−0.0277
in DMMP	−21	0.0245		

Conclusions

This study shows that simple organic field effect transistors respond to DMMP vapor thorugh changes in mobility, threshold voltage, and source−drain current. The devices exhibited a greater response to DMMP than to other interferent analytes we tested. We demonstrate for the first time that a device based

on a two-layer blend OFET has a higher sensitivity and shorter response time compared to the case of an unfunctionalized pure semiconductor serving as the active layer. All the responses have an obvious gate voltage dependence. Higher absolute current responses were observed at higher gate voltages, while the optimal gate voltages for the greatest relative responses were determined to be −20 V with our measurement. The two-layer blend has a significant response to the tens of ppm level of DMMP vapor. At optimal gate voltage, drain current decreased to less than 1% of its original value in a flow of diluted DMMP vapor, suggesting the capability of sensing ppb levels of analytes. The response times of the sensors can be shortened by reducing the film thickness. We plan to increase the Lewis and/or proton acidities of the surface groups on the OFETs, to increase the likelihood of effective adsorption of the analytes of actual interest, such as nerve gases, which are likely to be less basic than DMMP.

Acknowledgment. This work was performed with primary support from the National Science Foundation SENSORS program (Award No. 0528472). We also acknowledge support from The Johns Hopkins University Applied Physics Laboratory Partnership program. Helpful discussions with Professor Andreas Andreou are greatly appreciated.

JA068964Z